Applied Catalysis B: Environmental 325 (2023) 122325

Contents lists available at ScienceDirect

Applied Catalysis B: Environmental

journal homepage: www.elsevier.com/locate/apcatb

Anchoring catalytically active species on alumina via surface hydroxyl group for durable surface reaction

Yunji Choi [a], Gunjoo Kim [a], Jinwoong Kim [a], Seungwoo Lee [a], Jeong-Chul Kim [b], Ryong Ryoo [c], Hyunjoo Lee [a,*]

[a] Department of Chemical and Biomolecular Engineering, Korea Advanced Institute of Science and Technology, Daejeon 34141, the Republic of Korea
[b] Center for Nanomaterials and Chemical Reactions, Institute for Basic Science (IBS), Daejeon 34141, the Republic of Korea
[c] KENTECH Institute for Environmental and Climate Technology, Korea Institute of Energy Technology (KENTECH), Naju 58330, the Republic of Korea

ARTICLE INFO

Keywords:
Surface hydroxyl groups
Alumina
Ceria
Platinum
Durability

ABSTRACT

Ensuring durable catalyst structure is crucial for heterogeneous surface reactions. Particularly, exhaust gas treatment catalyst needs exceptional durability at very high temperature (≥ 800 °C) and low-temperature activity. Here, a hierarchical catalyst structure consisting of alumina, ceria, and Pt was synthesized to achieve high activity and durability. The alumina surface was modified to have surface hydroxyl groups by hydrothermal pre-treatment at various temperatures, then this alumina was used to anchor catalytically active species to form a highly durable surface structure. Whereas Pt and ceria on bare alumina suffered from significant sintering after aging at 800 °C, the same species formed on the pre-treated alumina hardly presented change in surface structure after aging. This durable $Pt/CeO_2/Al_2O_3$ catalyst showed no degradation for the simultaneous oxidation of CO, C_3H_6, and C_3H_8 with water vapor for repeated reactions or long-term reactions. This work can provide a useful guideline in designing a durable heterogeneous catalyst.

1. Introduction

Alumina is widely used in heterogeneous catalysts due to its excellent mechanical strength, high thermal stability, high surface area, and robust chemical inertness [1–3]. It finds its application in a variety of catalytic reactions, such as preferential oxidation of CO [4], methane combustion [5], water-gas shift reaction (WGS) [6], diesel oxidation catalytic reactions (DOC) [7], three-way catalytic reactions (TWC) [8], and NO_x-selective catalytic reduction (SCR) [9]. Typically, active metal species are dispersed on alumina support to reduce the use of expensive metal. Metal oxides are often dispersed on alumina as well because it can facilitate oxygen transfer or adsorb the reactants better [10]. Anchoring catalytically active species on support is a promising way to control the surface structure of the catalyst thus the catalytic properties [11,12]. Understanding the anchoring mechanism of active species on alumina support is important in order to design highly active and durable catalysts.

The complexity of crystal structure and chemical nature of alumina has made the extensive study on the alumina surface relatively difficult [13–15]. Some previous studies have reported anchoring sites on alumina that strongly bind metal or metal oxide to the alumina surface. The unsaturated pentacoordinate Al^{3+} (Al^{3+}_{penta}) sites, created by dehydration and dehydroxylation of alumina, were proposed to be anchoring sites of Pt on γ-Al_2O_3 [16,17]. Other metals such as Ru, Pd, Ni and Pt-Sn were immobilized on Al^{3+}_{penta} centers and demonstrated high activity for hydrogenation of aromatics, methane combustion, dry reforming of methane (DRM), and propane dehydrogenation [2,18–21]. In the case of metal oxide, WO_x was anchored on Al^{3+}_{penta} sites of γ-Al_2O_3 platelets, synthesized by calcination of γ-AlO(OH), and exhibited good activity for alkanol dehydration [22]. The BaO anchored on the Al^{3+}_{penta} sites could immobilize NO_x efficiently [23,24].

The surface hydroxyl groups on alumina support were also reported to anchor metal or metal oxide. Ag and Pt metal species were anchored on γ-Al_2O_3 by surface hydroxyl groups, resulting in high activity in NO_x-SCR, propane dehydrogenation, and formaldehyde oxidation [25–28]. Particularly, Ag single atoms could be immobilized via terminal hydroxyl groups on the alumina [26]. MoO_x and ReO_x were anchored by hydroxyl groups existing on γ-Al_2O_3 and used for olefin metathesis [29–31]. The inherent surface hydroxyl groups on the alumina were typically used as anchoring sites. Controlling the surface hydroxyl

* Corresponding author.
E-mail address: azhyun@kaist.ac.kr (H. Lee).

https://doi.org/10.1016/j.apcatb.2022.122325
Received 2 September 2022; Received in revised form 21 December 2022; Accepted 22 December 2022
Available online 23 December 2022
0926-3373/© 2022 Elsevier B.V. All rights reserved.

groups of alumina can provide a useful way to modulate the surface structure of the catalysts.

In this work, we created hydroxyl groups on γ-Al_2O_3 surface by hydrothermal pre-treatments. The surface hydroxyl groups were utilized as the anchoring sites for ceria species, and Pt was deposited, forming a hierarchical structure consisting of alumina, ceria nanodomain (≤ 10 nm), and Pt clusters (≤ 2 nm). The Pt/CeO_2/Al_2O_3 catalysts were tested for simultaneous catalytic oxidation of CO, C_3H_6, and C_3H_8 in the presence of water vapor, which typically exist in exhaust gas. Whereas the ceria domain on bare alumina sintered significantly after aging at 800 ºC with degraded reaction performance, the ceria on pre-treated alumina barely changed even after the aging, preserving the initial performance. With the hydroxyl group as anchoring sites, the catalysts could maintain their surface structure and demonstrated outstanding durability even after aging, repeated reactions, and long-term reactions.

2. Experimental section

2.1. Catalyst preparation

γ-Al_2O_3 was synthesized from aluminum nitrate ($Al(NO_3)_3{\cdot}9H_2O$; Sigma-Aldrich, ≥ 98%) and urea ($CO(NH_2)_2$; Sigma-Aldrich) by following the previous report [32]. The aluminum nitrate 6.44 g and urea 9.28 g were each dissolved in 50 mL of deionized water separately. After mixing these two solutions, the mixture was placed in a Teflon-lined stainless autoclave at 100 °C for 24 h. After cooling, the precipitate was filtered and washed multiple times with deionized water and ethanol. Then, the obtained sample was dried at 80 °C overnight, ground, and calcined at 750 °C for 5 h. The synthesized γ-Al_2O_3 was pre-treated by flowing 10% H_2O (air balance) at 500 °C or 750 °C for 10 h. Then, 1 wt% of Pt and 10, 20, or 30 wt% of ceria were deposited onto the alumina. The cerium precursor solution was prepared by adding an appropriate amount of $Ce(NO_3)_3{\cdot}6\ H_2O$ (Kanto chemical, 99.99%) in 4 mL of deionized water, and the alumina was introduced into the above solution at room temperature while stirring for 1 h. The Pt precursor solution including an appropriate amount of chloroplatinic acid ($H_2PtCl_6{\cdot}6H_2O$; Sigma-Aldrich, ≤100%) was added into a suspension of alumina powder in a cerium precursor solution. The resulting solution was heated at 80 °C until the complete evaporation. The powder was dried at 80 °C overnight in an oven, ground, and calcined at 500 °C for 5 h in static air. Lastly, the calcined powder was reduced at 500 °C for 2 h under 10% H_2 (N_2 balance). Chlorine in chloroplatinic acid was removed by calcination and reduction at 500 °C [33,34]. The synthesized catalysts were aged at 800 °C for 25 h under 10% water vapor (air balance) to test the durability. The aged catalyst was reduced at 500 °C for 2 h under 10% H_2 (N_2 balance). The catalysts were denoted as ^{x}A-yC-Pt-(a) (^{x}A indicates bare alumina (^{b}A), alumina pre-treated at 500 °C or 750 °C (^{500}A or ^{750}A); yC indicates ceria with weight% of y; Pt indicates 1 wt% of Pt impregnated; '-a′ is added when aging was conducted). For the Pt/Al_2O_3 catalyst, Pt was impregnated onto γ-Al_2O_3 without ceria impregnation. CeO_2 was synthesized by a conventional precipitation method. 1 g of $Ce(NO_3)_3{\cdot}6\ H_2O$ was dissolved in deionized water, and NH_4OH (ammonia water, Duksan, 30%) was used to reach pH of 8.5. After stirring for 4 h, the resulting product was filtered and washed with ethanol and deionized water. The precipitate was dried at 80 °C overnight, ground, and calcined in static air at 500 °C for 4 h. To form Pt/CeO_2 catalyst, Pt was impregnated to the CeO_2 support with the same method as Pt/CeO_2/Al_2O_3 catalysts.

2.2. Catalytic reactions

The simultaneous oxidation of CO, C_3H_6, and C_3H_8 was carried out in a fixed-bed quartz reactor. The reactor was loaded with 50 mg of catalyst. To remove any impurity, the reactor was heated at 100 °C for 1 h under 100 sccm of He gas and cooled to room temperature. The gas composition of 1% CO, 0.2% C_3H_6, 0.2% C_3H_8, 10% O_2, 5% H_2O in He balance at 120,000 mL g^{-1} h^{-1} was introduced, with a total of 100 sccm as feed gas. At atmospheric pressure, the temperature of the reactor was raised to a target temperature (ramping rate of 5 °C min^{-1}) and maintained at each temperature for 10 min to obtain a steady state. The outlet gases were analyzed in a thermal conductivity detector (TCD) and a flame ionization detector (FID) of a Younglin GC 6500 system online gas chromatography (GC) equipped with a packed bed column (Carboxen1000, SUPELCO) and a capillary column (GS-GASPRO, Agilent Technologies).

2.3. Characterizations

Diffuse reflectance infrared Fourier-transform spectroscopy (DRIFTS) was obtained using Nicolet iS-50 (Thermo Scientific) upon CO adsorption. Finely ground mixture of KBr and catalyst was transferred in a sample cup and placed inside a DRIFTS cell with a KBr window. The pre-treatment was performed at 100 °C for 1 h under Ar. After cooling down to room temperature under Ar flow, the feed gas of 2% CO (Ar balance) was introduced to the cell for 10 min, and DRIFT spectra were acquired under vacuum.

The powder X-ray diffraction (XRD) patterns were obtained by Bruker D2 Phaser instrument under Cu Kα radiation. Solid-state ^{1}H magic angle spinning (MAS) nuclear magnetic resonance (NMR) was performed using an Avance HD 400WB spectrometer (Bruker) operating at 400.13 MHz for ^{1}H at room temperature. Before measurement, samples were pre-treated under vacuum at 250 °C overnight. The solid-state ^{1}H MAS NMR data were obtained under the following conditions: 2.5 μs pulse width (single-pulse sequence), 5 s relaxation delay, 12 kHz spinning rate, and 100 acquisitions. The transmission electron microscopy (TEM) images were taken using a Talos F200X (FEI) with an accelerating voltage of 200 kV. The high angle annular dark field-scanning TEM (HAADF-STEM) images and the energy-dispersive X-ray spectroscopy (EDS) elemental mapping images were obtained using a Titan cubed G2 60–300 (FEI) operating at an accelerating voltage of 300 kV. STEM images with bright field (BF), dark field (DF), and secondary electron (SE) detectors were collected at 200 kV using a Hitachi HF5000. The Brunauer−Emmett−Teller (BET) surface area measurement was acquired from nitrogen adsorption using a Micromeritics Tristar II 3020. X-ray photoelectron spectroscopy (XPS) was taken using K-alpha (ThermoVG Scientific) to study the electronic property of Ce. The C 1 s peak at 284.8 eV was used as a reference in order to calibrate the binding energies.

A dispersion of Pt was measured by a CO chemisorption method with a BELCAT-B (MicrotracBEL) [35,36]. First, 50 mg of catalyst was heated at 300 °C for 10 min in 3.5% O_2 (He balance) and cooled down to 50 °C. Then, the catalyst was treated with He for 5 min and heated to 200 °C under 5% H_2 (Ar balance). After cooling down to 50 °C, following treatments were performed: (1) He for 5 min; (2) 3.5% O_2 (He balance) for 5 min; (3) CO_2 for 10 min; (4) He for 20 min; (5) 5% H_2 (Ar balance) for 5 min. CO_2 was pre-injected to prevent over-estimation by forming carbonates on ceria surface. CO-pulse was injected in a He stream every minute until the CO adsorption was saturated. H_2 temperature-programmed reduction (H_2-TPR) was performed on BELCAT-B (MicrotracBEL). The catalyst was heated with 50 sccm of Ar at 150 °C for 1 h and cooled down. Then, temperature was raised to 800 °C under 5% H_2 (Ar balance) gas at a ramping rate of 10 °C min^{-1}.

3. Results and discussion

3.1. Effect of surface hydroxyl groups on γ-Al_2O_3

While alumina has been used as a support for various gas-phase reactions, ceria has been often loaded on the alumina as auxiliary materials to facilitate oxygen transfer for particularly oxidation reaction [37,38]. Here, we synthesize Pt/CeO_2/Al_2O_3 catalysts by depositing catalytically active species of ceria and Pt on γ-Al_2O_3. To observe the effect of

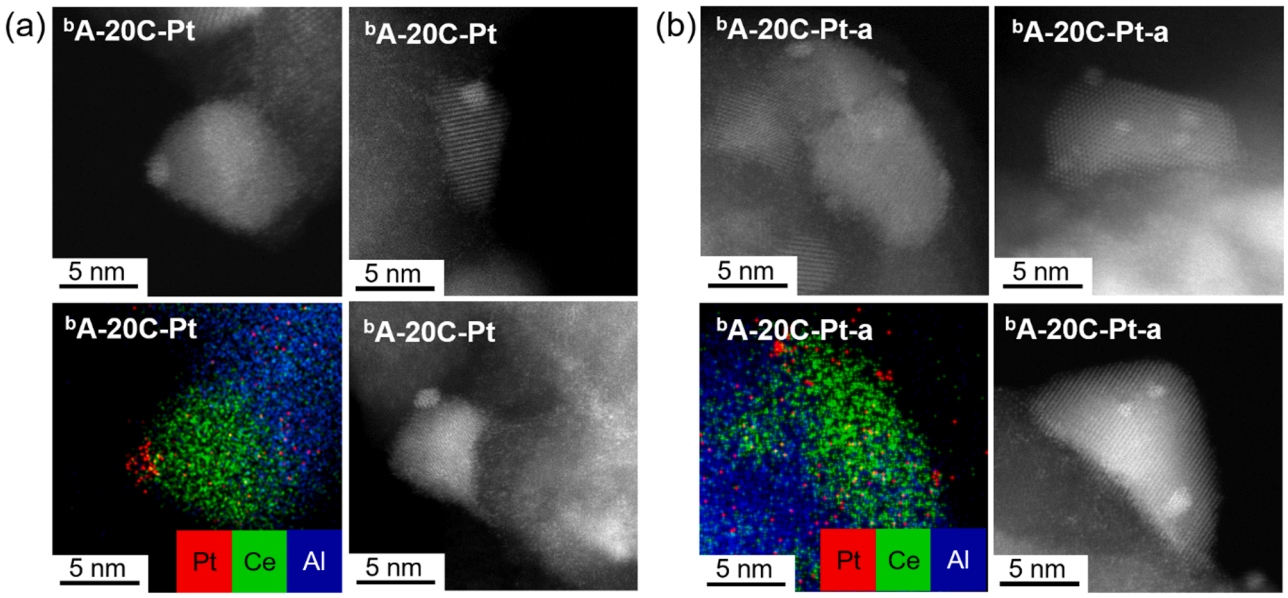

Fig. 1. Morphology of ^{b}A-20C-Pt before and after aging. HAADF-STEM images and EDS mapping images of (a) ^{b}A-20C-Pt and (b) ^{b}A-20C-Pt-a. (^{b}A indicates bare alumina; 20C indicates ceria with 20 weight%; '-a' is added when hydrothermal aging was conducted).

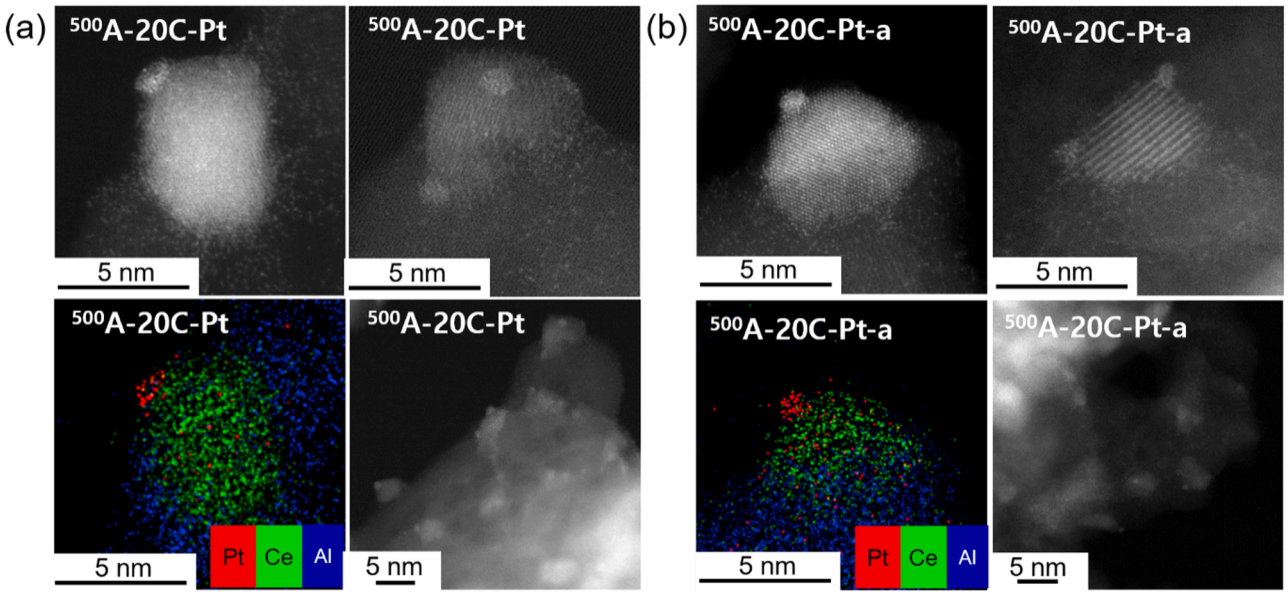

Fig. 2. Morphology of ^{500}A-20C-Pt before and after aging. HAADF-STEM images and EDS mapping images of (a) ^{500}A-20C-Pt and (b) ^{500}A-20C-Pt-a. (^{500}A indicates alumina pre-treated at 500 °C); 20C indicates ceria with 20 weight%; '-a' is added when hydrothermal aging was conducted).

alumina surface property on anchoring the catalytically active species, the bare alumina was used, denoted as ^{b}A, or the alumina pre-treated with 10% H_2O (air balance) at 500 °C or 750 °C was used, denoted as ^{500}A or ^{750}A, respectively. Fig. 1 and Fig. 2 show HAADF-STEM images and EDS mapping images of the $Pt/CeO_2/Al_2O_3$ before and after hydrothermal aging at 800 °C. ^{b}A-20C-Pt and ^{500}A-20C-Pt indicate the catalysts consisting of alumina with 20 wt% CeO_2 and 1 wt% Pt. As shown in Fig. 1a and Fig. 2a, their HAADF-STEM and EDS images clearly demonstrate the ceria domain formed on alumina and Pt atoms mostly anchored on ceria. On these catalysts, aging was performed by flowing 10% H_2O (air balance) at 800 °C for 25 h, denoted by adding '-a' in the catalyst name. Interestingly, ^{b}A-20C-Pt-a catalyst demonstrated significant sintering of ceria domain, whereas the ceria domain was barely changed in ^{500}A-20C-Pt-a, as shown in Fig. 1b and Fig. 2b. Fig. S1 shows STEM images from BF, DF, and SE detectors of ^{b}A-20C-Pt-a. Large ceria domains with $\geq$ 10 nm in size were observed after the aging. Notably, Pt clusters with $\leq$ 2 nm were observed, but SE-STEM image suggests that some of them might be located inside the ceria, not at the ceria surface. The clusters appeared in DF-STEM image, which were encircled with white line in Fig. S1b, were not observed in SE-STEM image (scanning mode) of Fig. S1c, implying that they might not be located at the surface, although we cannot exclude the possibility that they exist beneath the ceria domain. The alumina pre-treatment could ensure the preservation of ceria and Pt species after the aging.

The pre-treatment of alumina could form surface hydroxyl groups as confirmed by solid state ^{1}H MAS NMR in Fig. 3a. The ^{1}H MAS NMR peaks are deconvoluted into four peaks of μ1-OH (−0.2 ~ 0.1 ppm), μ2-OH (1.7 ~ 2.0 ppm), μ3-OH (4.3 ~ 6.8 ppm), and H-bond donors (≥10 ppm) as shown in Fig. S2. The μ1-OH, μ2-OH, and μ3-OH indicate terminal, doubly bridging, and triply bridging hydroxyl groups,

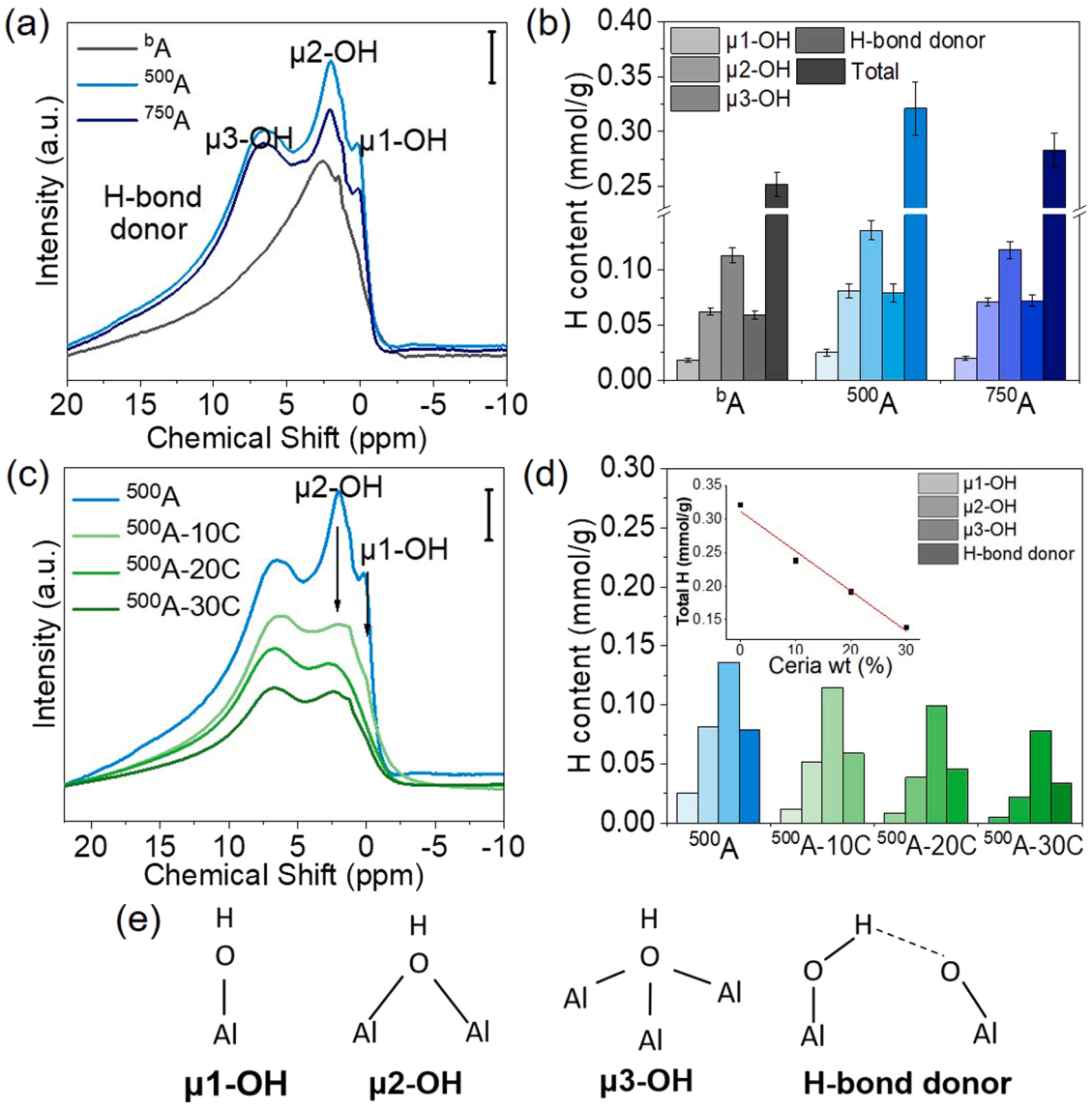

Fig. 3. (a) ^{1}H MAS NMR and (b) quantification of Al-OH group of ^{b}A, ^{500}A, and ^{750}A, (c) ^{1}H MAS NMR and (d) quantification of Al-OH group of ^{500}A and ^{500}A-yC (y = 10, 20, 30 wt%). Inset image represents total amount of Al-OH group for various ceria wt%. (e) Schematic drawing of μ1-OH, μ2-OH, μ3-OH, and H-bond donor.

respectively [21,39,40]. Schematic drawings of each Al-OH groups are shown in Fig. 3e [41,42]. The amount of Al-OH groups was quantified in Fig. 3b by using octakis(trimethylsiloxy)-silesquioxane, widely known as Q8M8, as the quantitation standard [40]. The amount of the hydroxyl groups was compared for ^{b}A, ^{500}A, and ^{750}A. The amount of hydroxyl groups increased from 0.25 mmol/g for ^{b}A to 0.32 mmol/g for ^{500}A and 0.28 mmol/g for ^{750}A after the pre-treatments. While the data in Fig. 3a were obtained after dehydration in order to exclude H resulting from adsorbed H_2O, ^{1}H MAS NMR results obtained without dehydration were also shown in Fig. S3. The amount of hydroxyl groups was estimated to be 0.51 mmol/g in ^{b}A, 0.59 mmol/g in ^{500}A, and 0.57 mmol/g in ^{750}A, which are larger than the values estimated with dehydration. In both cases, the pre-treatment at 500 °C resulted in the maximum amount of surface hydroxyl groups, compared to other pre-treatments.

XRD patterns in Fig. S4a confirmed that γ-Al_2O_3 crystalline structure was preserved even after the pre-treatment at 750 °C. TEM images in Fig. S4b-d revealed the rod-like morphology for ^{b}A, which exhibited little change after the pre-treatment at 500 and 750 °C. The values of the surface area measured by Brunauer-Emmett-Teller (BET) analysis were 136.4 m^2/g for ^{b}A, 88.7 m^2/g for ^{500}A, and 64.9 m^2/g for ^{750}A. When the OH density was estimated from H content in Fig. 3b and the surface area, it was 1.1 OH/nm^2 in ^{b}A, 2.2 OH/nm^2 in ^{500}A, and 2.6 OH/nm^2 in ^{750}A. ^{27}Al MAS NMR data in Fig. S5 show that the Al^{3+}_{penta} sites were detected with a peak at 38 ppm in ^{b}A while the peak disappeared after the hydrothermal pre-treatment.

Various amounts of ceria (10, 20, and 30 wt%) were deposited on alumina and analyzed with ^{1}H MAS NMR (Fig. 3c, Fig. S6a-d). The ^{1}H MAS NMR spectra showed a linear decrease in the amount of total hydroxyl groups as the ceria loading increased (Fig. 3d inset). The surface hydroxyl groups might also be formed on ceria surface, but these peaks are indistinguishable from the hydroxyl groups on alumina surface [43]. Particularly, the amount of terminal (μ1-OH) and doubly bridging hydroxyl group (μ2-OH) decreased significantly when 10 wt% of ceria was deposited to ^{500}A. The further increase of the ceria content resulted in less significant decrease in the amount of hydroxyl groups. These results could imply that the anchoring of ceria was achieved by terminal and bridging hydroxyl groups. The ceria would be initially impregnated on the hydroxyl groups on the alumina surface and grow into nanoparticles on alumina. The ^{1}H MAS NMR was also observed after impregnating both Pt and ceria on the pre-treated alumina. As shown in Fig. S6e, ^{1}H MAS NMR spectra demonstrated no significant distinction compared to spectra obtained without Pt, implying that ceria, not Pt, was anchored

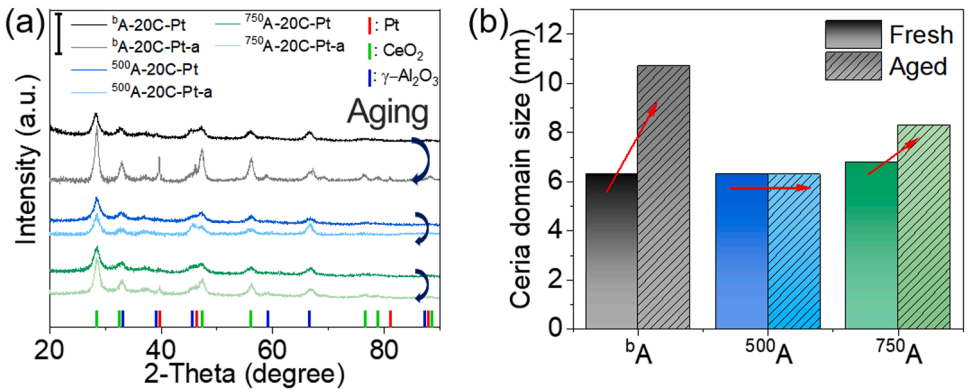

Fig. 4. (a) XRD patterns of ^{x}A-20C-Pt (x = b, 500 °C, 750 °C) before and after aging at 800 °C for 25 h with 10% H_2O (air balance). (b) ceria domain size estimated from CeO_2 (111) peak at 28.5°.

Table 1
Ceria domain size, surface area, and Pt dispersion of $Pt/CeO_2/Al_2O_3$ before and after aging at 800 °C for 25 h with 10% H_2O (air balance).

Sample	Ceria size (nm)[a]	BET surface area (m^2/g)	Pt dispersion (%)[b]
^{b}A	-	136.4	-
^{500}A	-	88.7	-
^{750}A	-	64.9	-
^{b}A-10C-Pt	3.7	104.9	59.9
^{b}A-10C-Pt-a	10.3	53.6	13.8
^{500}A-10C-Pt	3.9	69.1	58.1
^{500}A-10C-Pt-a	5.3	64.6	20.3
^{750}A-10C-Pt	4.1	56.2	58.8
^{750}A-10C-Pt-a	7.8	48.4	15.4
^{b}A-20C-Pt	6.3	97.1	50.6
^{b}A-20C-Pt-a	10.7	46.6	10.2
^{500}A-20C-Pt	6.3	58.6	78.5
^{500}A-20C-Pt-a	6.3	58.3	76.6
^{750}A-20C-Pt	6.8	53.9	74.4
^{750}A-20C-Pt-a	8.3	47.3	34.3
^{b}A-30C-Pt	6.4	78.5	51.2
^{b}A-30C-Pt-a	15.3	41.8	25.1
^{500}A-30C-Pt	6.4	56.5	66.4
^{500}A-30C-Pt-a	6.6	56.3	59.7
^{750}A-30C-Pt	6.8	49.8	68.4
^{750}A-30C-Pt-a	7.3	43.5	55.0
Pt/Al_2O_3	-	105.6	24.8
Pt/Al_2O_3-a	-	98.4	12.0
Pt/CeO_2	10.6	53.9	20.4
Pt/CeO_2-a	13.2	48.6	15.8

[a] Ceria domain size measured from CeO_2 (111) peak at 28.5°.
[b] The Pt dispersion was obtained by pulsed CO chemisorption.

on the alumina surface by hydroxyl groups.

3.2. Characterizations before and after aging

The structure of Pt and ceria supported on γ-Al_2O_3 was investigated in more detail to analyze the effect of surface hydroxyl groups. The catalysts were aged under 10% H_2O (air balance) flow at 800 °C for 25 h, and reduced under 10% H_2 (N_2 balance) flow at 500 °C for 2 h before the characterizations and reactions. Fig. 4a shows XRD patterns in which peaks were assigned to Pt, CeO_2, and γ-Al_2O_3. Ceria domain size was estimated from the CeO_2 (111) peak at 28.5°. Before the aging, ceria domain sizes of ^{b}A-20C-Pt, ^{500}A-20C-Pt, and ^{750}A-20C-Pt were similar as 6.3 nm, 6.3 nm, and 6.8 nm, respectively, regardless of alumina pre-treatment condition. After the aging, however, the ceria domain of ^{b}A-20C-Pt became significantly larger to 10.7 nm, whereas ^{500}A-20C-Pt had no change and ^{750}A-20C-Pt was observed with a slight increase to 8.3 nm (Fig. 4b). XRD patterns were also obtained for different ceria content of 10 and 30 wt% (Fig. S7a and S7c). Table 1 shows the change in the ceria domain size after the aging for various

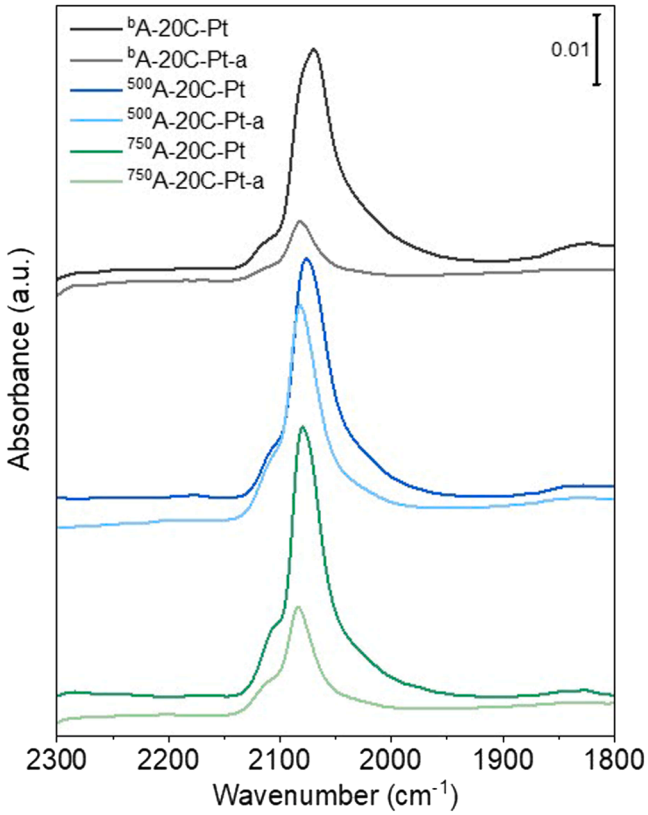

Fig. 5. DRIFT spectra of ^{x}A-20C-Pt (x = b, 500 °C, 750 °C) before and after aging at 800 °C 25 h with 10% H_2O (air balance).

samples. Whereas the ceria deposited on bare alumina demonstrated significant sintering, the ceria on pre-treated alumina showed only mild sintering. The changes in BET surface areas were also shown in Table 1. Clearly, the surface hydroxyl group formed on alumina could anchor ceria and suppress the sintering in spite of high temperature hydrothermal aging. Notably, ^{750}A had higher OH density than ^{500}A, but ceria sintering occurred more, possibly due to smaller surface area. The distance between ceria domains was smaller, causing more ceria sintering.

The Pt dispersion was measured using CO chemisorption to compare the Pt structure before and after the aging (Table 1). Pt dispersion decreased significantly from 50.6% to 10.2% for ^{b}A-20C-Pt after aging, whereas the dispersion barely decreased from 78.5% to 76.6% for ^{500}A-20C-Pt. The catalysts with different ceria contents of 10 wt% and 30 wt % also showed the same trend for Pt dispersion. DRIFT spectra were

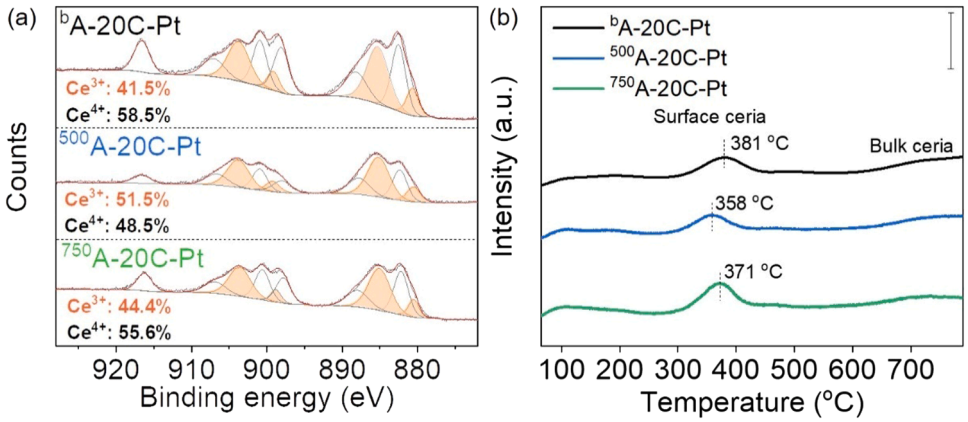

Fig. 6. (a) XPS Ce 3d spectra and (b) H_2-TPR of ^{x}A-20C-Pt (x = b, 500 °C, 750 °C).

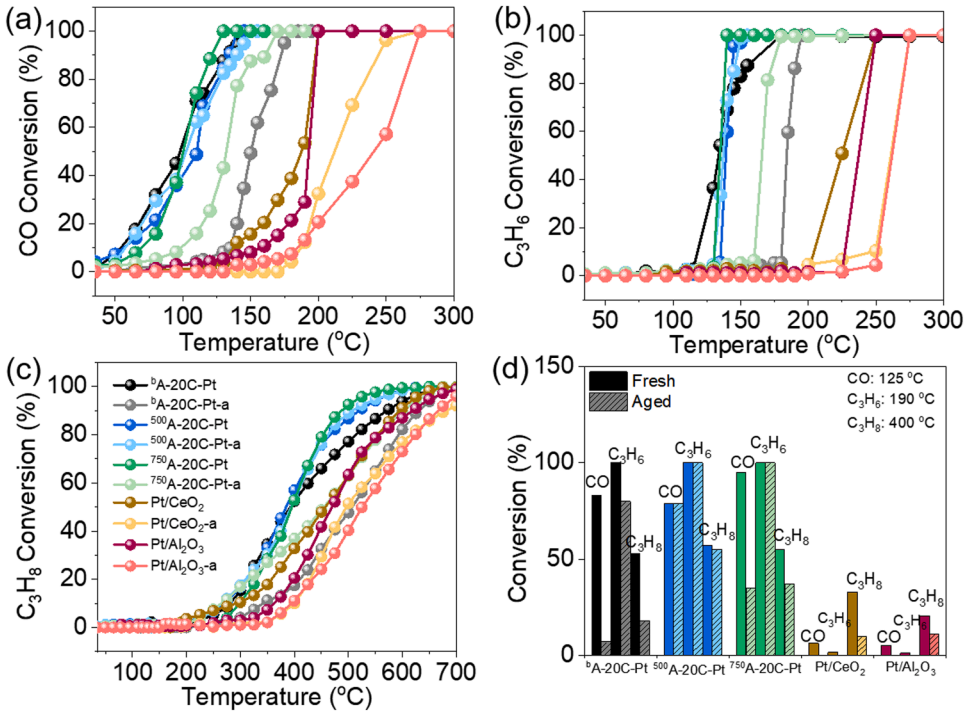

Fig. 7. Simultaneous oxidation of CO, C_3H_6, and C_3H_8 before and after aging. (a) CO conversion, (b) C_3H_6 conversion, (c) C_3H_8 conversion, (d) The changes in the conversion of CO, C_3H_6, and C_3H_8 (at 125 °C for CO, 190 °C for C_3H_6, 400 °C for C_3H_8) of ^{x}A-20C-Pt (x = b, 500 °C, 750 °C). Pt/CeO_2 and Pt/Al_2O_3 catalysts were also tested. The reactions were performed under 1% CO, 0.2% C_3H_6, 0.2% C_3H_8, 10% O_2, 5% H_2O in He balance at 120,000 mL g^{-1} h^{-1}. The aging was conducted at 800 °C for 25 h with 10% H_2O (air balance).

obtained before and after the aging. Fig. 5 shows that ^{b}A-20C-Pt, ^{500}A-20C-Pt, and ^{750}A-20C-Pt possess nearly identical Pt structure. The bridge bonded peak at 1825 cm^{-1}, typically indicating Pt nanoparticles [44,45], was small, instead a linear CO peak at 2078 cm^{-1}, which is observed for Pt clusters [46], was mainly obtained. After the aging, the Pt peaks in ^{b}A-20C-Pt-a presented a significant decrease in intensity, but the intensity for ^{500}A-20C-Pt-a remained nearly the same. The catalysts with different ceria contents also showed the same trend (Fig. S7b and S7d). When the ceria was firmly anchored on the alumina, Pt surface structure also hardly changed preserving its initial high dispersion. Interestingly, although Pt dispersion decreased significantly after the aging, small Pt clusters with ≤ 2 nm were still observed from STEM images for samples prepared on bare alumina. Pt clusters might be occluded inside the ceria upon ceria sintering, losing its exposure to gas-phase. The decrease in Pt dispersion might result from not only Pt sintering, but also from Pt inclusion inside the ceria upon ceria sintering.

The fraction of Ce^{3+} to Ce^{4+} was estimated from XPS spectra (Fig. 6a). While Ce^{4+} is observed in fully oxidized ceria, Ce^{3+} indicates oxygen defect sites [47,48]. These ceria defect sites are well known to stabilize Pt atoms efficiently [49,50]. While the Ce^{3+} fraction was 51.5% in ^{500}A-20C-Pt, it was 44.4% in ^{750}A-20C-Pt and 41.5% in ^{b}A-20C-Pt. XPS spectra were also obtained for different ceria contents in Fig. S8. H_2-TPR results showed the same trend for the surface redox property (Fig. 6b). The surface oxygen was reduced at 358 °C in ^{500}A-20C-Pt, while it was reduced at higher temperatures of 381 °C in ^{b}A-20C-Pt and 371 °C in ^{750}A-20C-Pt. H_2-TPR results for different ceria contents can be found in Fig. S9. The ceria formed on ^{500}A had the most defective surface, anchoring Pt more strongly, resulting in better durability.

3.3. Reaction performance

The $Pt/CeO_2/Al_2O_3$ catalysts were evaluated for simultaneous oxidation of CO, C_3H_6, and C_3H_8 with water vapor. The gas composition was 1% CO, 0.2% C_3H_6, 0.2% C_3H_8, 10% O_2, and 5% H_2O in He balance. Fig. 7 shows the conversions of CO, C_3H_6, and C_3H_8 obtained before and after the aging. The ^{b}A-20C-Pt, ^{500}A-20C-Pt, and ^{750}A-20C-Pt demonstrated similar activity, in accordance with their similar ceria and Pt properties. However, after the aging at 800 °C, the activity of ^{b}A-20C-Pt

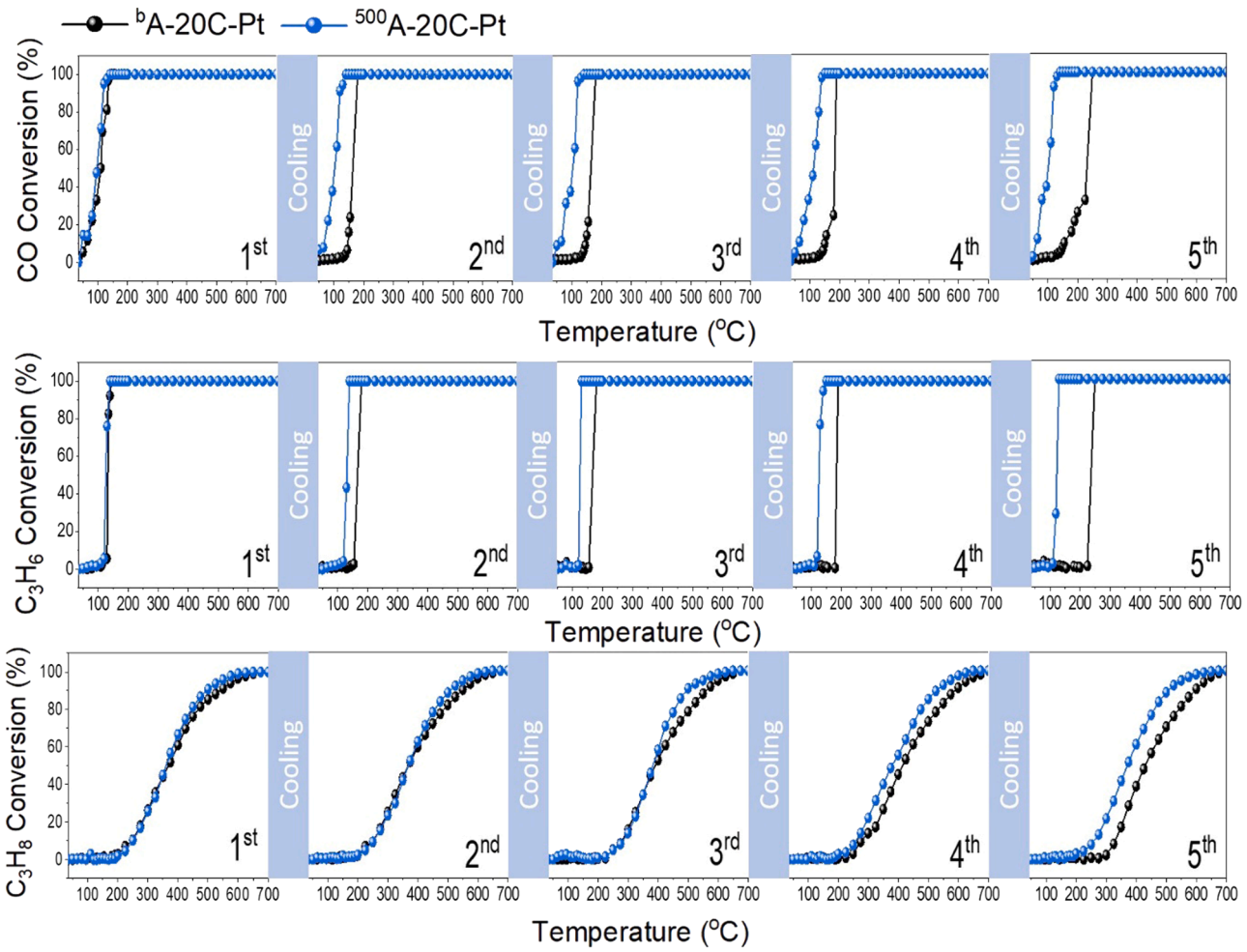

Fig. 8. Repeated reactions of ^{b}A-20C-Pt and ^{500}A-20C-Pt for 5 cycles. The reactions were performed under 1% CO, 0.2% C_3H_6, 0.2% C_3H_8, 10% O_2, 5% H_2O in He balance at 120,000 mL g^{-1} h^{-1}.

dropped significantly, while the activity of ^{500}A-20C-Pt remained unchanged. Fig. 7d summarizes these changes by comparing the conversions before and after the aging at 125 °C for CO, at 190 °C for C_3H_6, and at 400 °C for C_3H_8. The conversions of CO, C_3H_6, and C_3H_8 dropped from 83%, 100%, and 53% to 7%, 80%, and 18%, respectively, in ^{b}A-20C-Pt, whereas the conversions hardly changed from 79%, 100%, and 57% to 79%, 100%, and 55% in ^{500}A-20C-Pt. The different ceria loadings of 10 wt% and 30 wt% were tested for the simultaneous oxidation (Fig. S10), and they showed the same trend as 20 wt%. Even after aging at 1000 °C, ^{500}A-20C-Pt presented a good performance where ^{b}A-20C-Pt lost its activity significantly (Fig. S11). The Pt/CeO_2 and Pt/Al_2O_3 catalysts were also prepared with 1 wt% of Pt, and their catalytic performance was compared with Pt/CeO_2/Al_2O_3 catalysts. The Pt/CeO_2 and Pt/Al_2O_3 catalysts presented much poorer Pt dispersion and catalytic activity than Pt/CeO_2/Al_2O_3 catalysts. The hierarchically structured Pt/CeO_2/Al_2O_3 catalysts, in which defective CeO_2 was anchored on Al_2O_3 and provided anchoring sites for Pt, presented much better activity and durability. When the amount of surface hydroxyl groups on alumina was further diminished by calcining the alumina at 500 °C, the ceria domain became even larger than the catalysts formed on bare alumina (Fig. S12). Also, the activity after aging became much poorer, indicating the effect of the surface hydroxyl groups on anchoring (Fig. S13). The ceria firmly anchored on alumina did not suffer from sintering, also preserving surface Pt structure. This durable surface structure presented a superior activity and durability for the simultaneous oxidation after the aging at 800 °C.

To evaluate the effect of Pt inclusion, the ceria was deposited on bare alumina and hydrothermally aged at 800 °C, then Pt was deposited. When the reaction performance was compared before and after additional aging at 800 °C, the decrease in the activity was rather minimal (Fig. S14), indicating that the degradation in performance of ^{b}A-20C-Pt mainly resulted from ceria sintering. Pt inclusion induced by ceria sintering caused the degradation.

The catalytic durability of ^{b}A-20C-Pt and ^{500}A-20C-Pt catalysts was further investigated for repeated reactions of the simultaneous oxidation as shown in Fig. 8. The reaction temperature was raised to 700 °C and then cooled down to room temperature. This procedure was repeated for five times. Upon repeated reaction cycles, ^{b}A-20C-Pt clearly exhibited the degradation in the conversions of CO, C_3H_6, and C_3H_8. However, ^{500}A-20C-Pt presented no change in conversions over five cycles.

The long-term reactions were also conducted for 70 h for ^{b}A-20C-Pt and ^{500}A-20C-Pt (Fig. 9). The reaction was performed at 140 °C to observe the change in CO and C_3H_6 conversions, while the reaction at 300 °C was conducted to observe the change in C_3H_8 conversion. The ^{500}A-20C-Pt barely exhibited change in the conversions of CO, C_3H_6, and C_3H_8, but the ^{b}A-20C-Pt showed the degradation in the conversions. The structure of ^{b}A-20C-Pt and ^{500}A-20C-Pt were examined by DRIFTS after 70 h at 300 °C (Fig. 9d). The CO peak intensity decreased greatly in the ^{b}A-20C-Pt to unnoticeable size, whereas the peak remained unchanged in the ^{500}A-20C-Pt. The ceria sintered and cokes were formed on ^{b}A-20C-Pt unlike ^{500}A-20C-Pt (Fig. S15). When the ceria was strongly anchored on the alumina via surface hydroxyl groups, the catalyst surface was very durable with no degradation upon hydrothermal aging at 800 °C, repeated reactions, and long-term reactions.

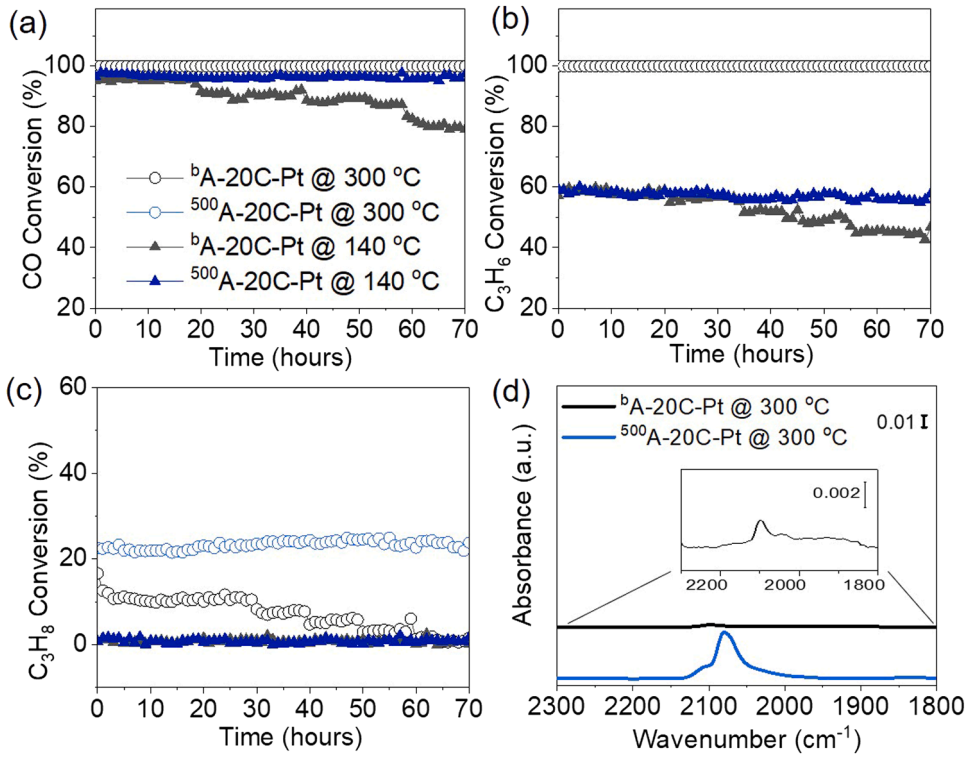

Fig. 9. (a-c) Long-term reactions of ^{b}A-20C-Pt and ^{500}A-20C-Pt at 140 °C and 300 °C. The reactions were performed under 1% CO, 0.2% C_3H_6, 0.2% C_3H_8, 10% O_2, 5% H_2O in He balance at 120,000 mL g^{-1} h^{-1}. (d) DRIFT spectra of ^{b}A-20C-Pt and ^{500}A-20C-Pt after the long-term reactions at 300 °C. The inset image indicates the magnification of DRIFT spectra on ^{b}A-20C-Pt.

4. Conclusions

γ-Al_2O_3 was pre-treated to create surface hydroxyl groups, then ceria and Pt were deposited on the alumina. When this catalyst was compared with the catalyst deposited on bare alumina, the ceria nanodomain formed on pre-treated alumina, which had ~ 6 nm in size, was preserved after aging at 800 ºC, but the ceria on bare alumina sintered significantly to ≥ 10 nm after the aging. ^{1}H MAS NMR showed that the ceria was mainly anchored by terminal and bridging hydroxyl groups. When different ceria loadings of 10, 20, and 30 wt% were tested, 20 wt% showed the highest durability after the aging at 800 ºC. Pt dispersion and DRIFTS results also showed that surface Pt structure was preserved when ceria was anchored onto the pre-treated alumina. When Pt/CeO_2/Al_2O_3 catalysts were tested for the simultaneous oxidation of CO, C_3H_6, and C_3H_8 with water vapor, the anchored catalyst on pre-treated alumina presented high activity and durability, whereas the catalyst on bare alumina suffered from significant degradation after the aging at 800 ºC. The anchored catalyst presented superior durability even for repeated reactions and long-term reactions. This hierarchical heterogeneous catalyst, in which ceria is anchored on alumina and Pt is anchored on ceria defect sites, can be highly active and durable for high temperature gas-phase reactions.

CRediT authorship contribution statement

Yunji Choi: Conceptualization, Methodology, Investigation, Validation, Writing – original draft, Visualization. **Gunjoo Kim:** Investigation. **Jinwoong Kim:** Investigation. **Seungwoo Lee:** Investigation. **Jeong-Chul Kim:** Investigation, Methodology. **Ryong Ryoo:** Validation. **Hyunjoo Lee:** Conceptualization, Supervision, Project administration, Funding acquisition, Writing – review & editing.

Declaration of Competing Interest

The authors declare that they have no known competing financial interests or personal relationships that could have appeared to influence the work reported in this paper.

Data Availability

Data will be made available on request.

Acknowledgements

This research was supported by the National Research Foundation of Korea (NRF - 2016R1A5A1009592; 2019M3D1A1079306; 2021R1A3B1076715). We also appreciate KARA (KAIST Analysis center for Research Advancement) for characterization equipment.

Appendix A. Supporting information

Supplementary data associated with this article can be found in the online version at doi:10.1016/j.apcatb.2022.122325.

References

[1] M. Trueba, S.P. Trasatti, γ-Alumina as a support for catalysts: a review of fundamental aspects, Eur. J. Inorg. Chem. 2005 (2005) 3393–3403.
[2] X. Yang, Q. Li, E. Lu, Z. Wang, X. Gong, Z. Yu, Y. Guo, L. Wang, Y. Guo, W. Zhan, J. Zhang, S. Dai, Taming the stability of Pd active phases through a compartmentalizing strategy toward nanostructured catalyst supports, Nat. Commun. 10 (2019) 1611.
[3] S. He, T. Huang, Y. Fan, Tetradecylamine-induced assembly of Mo and Al precursors to prepare efficient NiMoS/Al_2O_3 catalysts for ultradeep hydrodesulfurization, Appl. Catal. B: Environ. 317 (2022), 121801.
[4] K. Sato, S. Zaitsu, G. Kitayama, S. Yagi, Y. Kayada, Y. Nishida, Y. Wada, K. Nagaoka, Operando spectroscopic study of the dynamics of Ru catalyst during preferential oxidation of CO and the prevention of ammonia poisoning by Pt, JACS Au 2 (2022) 1627–1637.

[5] Z. Liu, G. Xu, L. Zeng, W. Shi, Y. Wang, Y. Sun, Y. Yu, H. He, Anchoring Pt-doped PdO nanoparticles on γ-Al_2O_3 with highly dispersed La sites to create a methane oxidation catalyst, Appl. Catal. B: Environ. 324 (2023), 122259.

[6] T.R. Reina, S. Ivanova, M.A. Centeno, J.A. Odriozola, Boosting the activity of a Au/CeO_2/Al_2O_3 catalyst for the WGS reaction, Catal. Today 253 (2015) 149–154.

[7] A. Boubnov, S. Dahl, E. Johnson, A.P. Molina, S.B. Simonsen, F.M. Cano, S. Helveg, L.J. Lemus-Yegres, J.-D. Grunwaldt, Structure–activity relationships of Pt/Al_2O_3 catalysts for CO and NO oxidation at diesel exhaust conditions, Appl. Catal. B: Environ. 126 (2012) 315–325.

[8] H. Asakura, S. Hosokawa, T. Ina, K. Kato, K. Nitta, K. Uera, T. Uruga, H. Miura, T. Shishido, J. Ohyama, A. Satsuma, K. Sato, A. Yamamoto, S. Hinokuma, H. Yoshida, M. Machida, S. Yamazoe, T. Tsukuda, K. Teramura, T. Tanaka, Dynamic behavior of Rh Species in Rh/Al_2O_3 model catalyst during three-way catalytic reaction: an operando X-ray absorption spectroscopy study, J. Am. Chem. Soc. 140 (2018) 176–184.

[9] C.-J. Yoo, A. Getsoian, A. Bhan, NH_3 formation pathways from NO reduction by CO in the presence of water over Rh/Al_2O_3, Appl. Catal. B: Environ. 286 (2021), 119893.

[10] B.M. Reddy, K.N. Rao, G.K. Reddy, A. Khan, S.-E. Park, Structural characterization and oxidehydrogenation activity of CeO_2/Al_2O_3 and V_2O_5/CeO_2/Al_2O_3 catalysts, J. Phys. Chem. C. 111 (2007) 18751–18758.

[11] J. Oh, Y. Jo, T.W. Kim, H.B. Bathula, S. Yang, J.H. Baik, Y.-W. Suh, Highly efficient and robust Pt ensembles on mesoporous alumina for reversible H_2 charge and release of commercial benzyltoluene molecules, Appl. Catal. B: Environ. 305 (2022), 121061.

[12] M.J. Islam, M. Granollers Mesa, A. Osatiashtiani, J.C. Manayil, M.A. Isaacs, M. J. Taylor, S. Tsatsos, G. Kyriakou, PdCu single atom alloys supported on alumina for the selective hydrogenation of furfural, Appl. Catal. B: Environ. 299 (2021), 120652.

[13] K. Sohlberg, S.J. Pennycook, S.T. Pantelides, The bulk and surface structure of γ-Alumina, Chem. Eng. Commun. 181 (2000) 107–135.

[14] M. Corral Valero, P. Raybaud, P. Sautet, Influence of the hydroxylation of γ-Al_2O_3 surfaces on the stability and diffusion of single Pd atoms: a DFT study, J. Phys. Chem. B 110 (2006) 1759–1767.

[15] Y. Li, C.M. Lousada, P.A. Korzhavyi, The nature of hydrogen in γ-alumina, J. Appl. Phys. 115 (2014), 203514.

[16] J.H. Kwak, J. Hu, D. Mei, C.-W. Yi, D.H. Kim, C.H.F. Peden, L.F. Allard, J. Szanyi, Coordinatively unsaturated Al^{3+} centers as binding sites for active catalyst phases of platinum on γ-Al_2O_3, Science 325 (2009) 1670–1673.

[17] D. Mei, J.H. Kwak, J. Hu, S.J. Cho, J. Szanyi, L.F. Allard, C.H.F. Peden, Unique role of anchoring penta-coordinated Al^{3+} sites in the sintering of γ-Al_2O_3-supported Pt catalysts, J. Phys. Chem. Lett. 1 (2010) 2688–2691.

[18] N. Tang, Y. Cong, Q. Shang, C. Wu, G. Xu, X. Wang, Coordinatively unsaturated Al^{3+} sites anchored subnanometric ruthenium catalyst for hydrogenation of aromatics, ACS Catal. 7 (2017) 5987–5991.

[19] K. Murata, T. Shiotani, J. Ohyama, R. Wakabayashi, H. Maruoka, T. Kimura, A. Satsuma, Relationship between penta-coordinated Al^{3+} sites in the Al_2O_3 supports and CH_4 combustion activity of Pd/Al_2O_3 catalysts, Catal. Sci. Technol. 11 (2021) 2374–2378.

[20] L. Shi, G.-M. Deng, W.-C. Li, S. Miao, Q.-N. Wang, W.-P. Zhang, A.-H. Lu, Al_2O_3 nanosheets rich in pentacoordinate Al^{3+} ions stabilize Pt-Sn clusters for propane dehydrogenation, Angew. Chem. Int. Ed. 54 (2015) 13994–13998.

[21] Y. Zhang, Y. Zu, D. He, J. Liang, L. Zhu, Y. Mei, Y. Luo, The tailored role of "defect" sites on γ-alumina: a key to yield an efficient methane dry reforming catalyst with superior nickel utilization, Appl. Catal. B: Environ. 315 (2022), 121539.

[22] D. Shi, H. Wang, L. Kovarik, F. Gao, C. Wan, J.Z. Hu, Y. Wang, WO_x supported on γ-Al_2O_3 with different morphologies as model catalysts for alkanol dehydration, J. Catal. 363 (2018) 1–8.

[23] J.H. Kwak, J.Z. Hu, D.H. Kim, J. Szanyi, C.H.F. Peden, Penta-coordinated Al^{3+} ions as preferential nucleation sites for BaO on γ-Al_2O_3: an ultra-high-magnetic field ^{27}Al MAS NMR study, J. Catal. 251 (2007) 189–194.

[24] J.H. Kwak, D. Mei, C.-W. Yi, D.H. Kim, C.H.F. Peden, L.F. Allard, J. Szanyi, Understanding the nature of surface nitrates in BaO/γ-Al_2O_3 NOx storage materials: a combined experimental and theoretical study, J. Catal. 261 (2009) 17–22.

[25] Z. Zhang, G. He, Y. Li, C. Zhang, J. Ma, H. He, Effect of hydroxyl groups on metal anchoring and formaldehyde oxidation performance of Pt/Al_2O_3, Environ. Sci. Technol. 56 (2022) 10916–10924.

[26] F. Wang, J. Ma, S. Xin, Q. Wang, J. Xu, C. Zhang, H. He, X. Cheng Zeng, Resolving the puzzle of single-atom silver dispersion on nanosized γ-Al_2O_3 surface for high catalytic performance, Nat. Commun. 11 (2020) 529.

[27] H. Kubota, S. Mine, T. Toyao, Z. Maeno, K.-I. Shimizu, Redox-Driven reversible structural evolution of isolated silver atoms anchored to specific sites on γ-Al_2O_3, ACS Catal. 12 (2022) 544–559.

[28] R.M. Mironenko, O.B. Belskaya, V.P. Talsi, T.I. Gulyaeva, M.O. Kazakov, A. I. Nizovskii, A.V. Kalinkin, V.I. Bukhtiyarov, A.V. Lavrenov, V.A. Likholobov, Effect of γ-Al_2O_3 hydrothermal treatment on the formation and properties of platinum sites in Pt/γ-Al_2O_3 catalysts, Appl. Catal. A: Gen. 469 (2014) 472–482.

[29] A. Chakrabarti, I.E. Wachs, Molecular structure–reactivity relationships for olefin metathesis by Al_2O_3-supported surface MoO_x sites, ACS Catal. 8 (2018) 949–959.

[30] S. Lwin, C. Keturakis, J. Handzlik, P. Sautet, Y. Li, A.I. Frenkel, I.E. Wachs, Surface ReO_x sites on Al_2O_3 and their molecular structure–reactivity relationships for olefin metathesis, ACS Catal. 5 (2015) 1432–1444.

[31] S. Vorakitkanvasin, S.K.N. Ayudhya, K. Suriye, P. Praserthdam, J. Panpranot, Enhanced metathesis activity of low loading Re_2O_7/Al_2O_3 catalysts for propylene production by using aluminum nitrate as Al_2O_3 precursor, Appl. Catal. A: Gen. 517 (2016) 39–46.

[32] E.J. Jang, J. Lee, H.Y. Jeong, J.H. Kwak, Controlling the acid-base properties of alumina for stable PtSn-based propane dehydrogenation catalysts, Appl. Catal. A: Gen. 572 (2019) 1–8.

[33] K. Kinoshita, K. Routsis, J.A.S. Bett, The thermal decomposition of platinum(II) and (IV) complexes, Thermochim. Acta 10 (1974) 109–117.

[34] N.K. Sahu, A. Prakash, D. Bahadur, Role of different platinum precursors on the formation and reaction mechanism of FePt nanoparticles and their electrocatalytic performance towards methanol oxidation, Dalton Trans. 43 (2014) 4892–4900.

[35] H. Jeong, G. Lee, B.-S. Kim, J. Bae, J.W. Han, H. Lee, Fully dispersed Rh ensemble catalyst to enhance low-temperature activity, J. Am. Chem. Soc. 140 (2018) 9558–9565.

[36] T. Takeguchi, S. Manabe, R. Kikuchi, K. Eguchi, T. Kanazawa, S. Matsumoto, W. Ueda, Determination of dispersion of precious metals on CeO_2-containing supports, Appl. Catal. A: Gen. 293 (2005) 91–96.

[37] H.N. Pham, A. DeLaRiva, E.J. Peterson, R. Alcala, K. Khivantsev, J. Szanyi, X.S. Li, D. Jiang, W. Huang, Y. Sun, P. Tran, Q. Do, C.L. DiMaggio, Y. Wang, A.K. Datye, Designing ceria/alumina for efficient trapping of platinum single atoms, ACS Sustain. Chem. Eng. 10 (2022) 7603–7612.

[38] B.-S. Kim, J. Bae, H. Jeong, C. Choe, H. Lee, Surface restructuring of supported nano-ceria for improving sulfur resistance, ACS Catal. 11 (2021) 7154–7159.

[39] A.T.F. Batista, D. Wisser, T. Pigeon, D. Gajan, F. Diehl, M. Rivallan, L. Catita, A.-S. Gay, A. Lesage, C. Chizallet, P. Raybaud, Beyond γ-Al_2O_3 crystallite surfaces: the hidden features of edges revealed by solid-state ^1H NMR and DFT calculations, J. Catal. 378 (2019) 140–143.

[40] G.J. Kennedy, M. Afeworki, D.C. Calabro, C.E. Chase, R.J. Smiley, 1H MAS NMR (Magic-Angle Spinning Nuclear Magnetic Resonance) techniques for the quantitative determination of hydrogen types in solid catalysts and supports, Appl. Spectrosc. 58 (2004) 698–704.

[41] M. Delgado, F. Delbecq, C.C. Santini, F. Lefebvre, S. Norsic, P. Putaj, P. Sautet, J.-M. Basset, Evolution of structure and of grafting properties of γ-Alumina with pretreatment temperature, J. Phys. Chem. C. 116 (2012) 834–843.

[42] E.C. Decanio, J.C. Edwards, J.W. Bruno, Solid-State ^1H MAS NMR characterization of γ-Alumina and modified γ-Aluminas, J. Catal. 148 (1994) 76–83.

[43] L. Gill, A. Beste, B. Chen, M. Li, A.K.P. Mann, S.H. Overbury, E.W. Hagaman, Fast MAS 1H NMR study of water adsorption and dissociation on the (100) surface of ceria nanocubes: a fully hydroxylated, hydrophobic ceria surface, J. Phys. Chem. C. 121 (2017) 7450–7465.

[44] A. Sápi, G. Halasi, J. Kiss, D.G. Dobó, K.L. Juhász, V.J. Kolcsár, Z. Ferencz, G. Vári, V. Matolin, A. Erdőhelyi, Á. Kukovecz, Z. Kónya, In situ DRIFTS and NAP-XPS exploration of the complexity of CO_2 hydrogenation over size-controlled Pt nanoparticles supported on mesoporous NiO, J. Phys. Chem. C. 122 (2018) 5553–5565.

[45] H. Jeong, O. Kwon, B.-S. Kim, J. Bae, S. Shin, H.-E. Kim, J. Kim, H. Lee, Highly durable metal ensemble catalysts with full dispersion for automotive applications beyond single-atom catalysts, Nat. Catal. 3 (2020) 368–375.

[46] X.I. Pereira-Hernández, A. DeLaRiva, V. Muravev, D. Kunwar, H. Xiong, B. Sudduth, M. Engelhard, L. Kovarik, E.J.M. Hensen, Y. Wang, A.K. Datye, Tuning Pt-CeO_2 interactions by high-temperature vapor-phase synthesis for improved reducibility of lattice oxygen, Nat. Commun. 10 (2019) 1358.

[47] P. Dutta, S. Pal, M.S. Seehra, Y. Shi, E.M. Eyring, R.D. Ernst, Concentration of Ce^{3+} and oxygen vacancies in cerium oxide nanoparticles, Chem. Mater. 18 (2006) 5144–5146.

[48] D. Shen, Z. Li, J. Shan, G. Yu, X. Wang, Y. Zhang, C. Liu, S. Lyu, J. Li, L. Li, Synergistic Pt-CeO_2 interface boosting low temperature dry reforming of methane, Appl. Catal. B: Environ. 318 (2022), 121809.

[49] Z. Jiang, M. Jing, X. Feng, J. Xiong, C. He, M. Douthwaite, L. Zheng, W. Song, J. Liu, Z. Qu, Stabilizing platinum atoms on CeO_2 oxygen vacancies by metal-support interaction induced interface distortion: Mechanism and application, Appl. Catal. B: Environ. 278 (2020), 119304.

[50] L. Nie, D. Mei, H. Xiong, B. Peng, Z. Ren, X.I.P. Hernandez, A. DeLaRiva, M. Wang, M.H. Engelhard, L. Kovarik, A.K. Datye, Y. Wang, Activation of surface lattice oxygen in single-atom Pt/CeO_2 for low-temperature CO oxidation, Science 358 (2017) 1419–1423.